J. Plasma Phys. (2018), *vol.* 84, 905840615

doi:10.1017/S0022377818001277

Stochastic proton heating by kinetic-Alfvén-wave turbulence in moderately high-β plasmas

Ian W. Hoppock[1,†], Benjamin D. G. Chandran[1], Kristopher G. Klein[2,3], Alfred Mallet[1,4] and Daniel Verscharen[1,5]

[1]Space Science Center, University of New Hampshire, Durham, NH, 03824, USA

[2]Lunar and Planetary Laboratory, University of Arizona, Tucson, AZ, 85719, USA

[3]CLASP, University of Michigan, Ann Arbor, MI, 48109, USA

[4]Space Sciences Laboratory, University of California, Berkeley, CA, 94720, USA

[5]Mullard Space Science Laboratory, University College London, Dorking, RH5 6NT, UK

(Received 27 September 2018; revised 21 November 2018; accepted 22 November 2018)

Stochastic heating refers to an increase in the average magnetic moment of charged particles interacting with electromagnetic fluctuations whose frequencies are smaller than the particles' cyclotron frequencies. This type of heating arises when the amplitude of the gyroscale fluctuations exceeds a certain threshold, causing particle orbits in the plane perpendicular to the magnetic field to become stochastic rather than nearly periodic. We consider the stochastic heating of protons by Alfvén-wave (AW) and kinetic-Alfvén-wave (KAW) turbulence, which may make an important contribution to the heating of the solar wind. Using phenomenological arguments, we derive the stochastic-proton-heating rate in plasmas in which $\beta_p \sim 1$–30, where β_p is the ratio of the proton pressure to the magnetic pressure. (We do not consider the $\beta_p \gtrsim 30$ regime, in which KAWs at the proton gyroscale become non-propagating.) We test our formula for the stochastic-heating rate by numerically tracking test-particle protons interacting with a spectrum of randomly phased AWs and KAWs. Previous studies have demonstrated that at $\beta_p \lesssim 1$, particles are energized primarily by time variations in the electrostatic potential and thermal-proton gyro-orbits are stochasticized primarily by gyroscale fluctuations in the electrostatic potential. In contrast, at $\beta_p \gtrsim 1$, particles are energized primarily by the solenoidal component of the electric field and thermal-proton gyro-orbits are stochasticized primarily by gyroscale fluctuations in the magnetic field.

Key words: astrophysical plasmas, plasma heating, space plasma physics

1. Introduction

In the mid-twentieth century several authors published hydrodynamic models of the solar wind that imposed a fixed temperature at the coronal base and took thermal

† Email address for correspondence: ian.hoppock@unh.edu

conduction to be the only heating mechanism (e.g. Parker 1958, 1965; Hartle & Sturrock 1968; Durney 1972). These models were unable to explain the high proton temperatures and fast-solar-wind speeds observed at a heliocentric distance r of 1 astronomical unit (au) for realistic values of the coronal temperature and density, indicating that the fast solar wind is heated primarily by some mechanism other than thermal conduction. Parker (1965) and Coleman (1968) proposed that Alfvén waves (AWs) and AW turbulence provide this additional heating. Support for this suggestion can be found in the many spacecraft observations of AW-like turbulence in the solar wind (see Belcher 1971; Tu & Marsch 1995; Bale *et al.* 2005), remote observations of AW-like fluctuations in the solar corona (see De Pontieu *et al.* 2007; Tomczyk *et al.* 2007) and the agreement between AW-driven solar-wind models and solar-wind temperature, density and flow-speed profiles (Cranmer, van Ballegooijen & Edgar 2007; Verdini *et al.* 2010; Chandran *et al.* 2011; van der Holst *et al.* 2014).

AWs oscillate at a frequency $\omega = k_\parallel v_\mathrm{A}$, where $k_\parallel$ ($k_\perp$) is the component of the wave vector $\boldsymbol{k}$ parallel (perpendicular) to the background magnetic field, $\boldsymbol{B}_0$, $v_\mathrm{A} = B_0/\sqrt{4\pi n_\mathrm{p} m}$ is the Alfvén speed, n_p is the proton number density and m is the proton mass.[1] In AW turbulence, interactions between counter-propagating AWs cause AW energy to cascade from larger to smaller scales. This energy cascade is anisotropic, in the sense that the small-scale AW 'eddies', or wave packets, generated by the cascade vary much more rapidly perpendicular to the magnetic field than along the magnetic field (e.g. Shebalin, Matthaeus & Montgomery 1983; Goldreich & Sridhar 1995; Cho & Vishniac 2000; Horbury, Forman & Oughton 2008; Podesta 2013; Chen 2016). As a consequence, within the inertial range (scales larger than the thermal-proton gyroradius ρ_th and smaller than the outer scale or driving scale), $\omega \ll \Omega$, where Ω is the proton cyclotron frequency. At $k_\perp \rho_\mathrm{th} \sim 1$, the AW cascade transitions to a kinetic-Alfvén-wave (KAW) cascade (Schekochihin *et al.* 2009).

Studies of the dissipation of low-frequency ($\omega \ll \Omega$), anisotropic, AW/KAW turbulence based on linear wave damping (e.g. Quataert 1998; Howes *et al.* 2008) conclude that AW/KAW turbulence leads mostly to parallel heating of the particles (i.e. heating that increases the speed of the thermal motions along $\boldsymbol{B}$). On the other hand, perpendicular ion heating is the dominant form of heating in the near-Sun solar wind (Esser *et al.* 1999; Marsch 2006; Cranmer *et al.* 2009; Hellinger *et al.* 2013). This discrepancy suggests that AW/KAW turbulence in the solar wind dissipates via some nonlinear mechanism (e.g. Dmitruk, Matthaeus & Seenu 2004; Markovskii *et al.* 2006; Lehe, Parrish & Quataert 2009; Schekochihin *et al.* 2009; Chandran *et al.* 2010; Servidio *et al.* 2011; Lynn *et al.* 2012; Xia *et al.* 2013; Kawazura, Barnes & Schekochihin 2018). This suggestion is supported by studies that find a correlation between ion temperatures and fluctuation amplitudes in solar-wind measurements and numerical simulations (e.g. Wu *et al.* 2013; Grošelj *et al.* 2017; Hughes *et al.* 2017; Vech, Klein & Kasper 2018).

In this paper, we consider one such nonlinear mechanism: stochastic heating. In stochastic proton heating, AW/KAW fluctuations at the proton gyroscale have sufficiently large amplitudes that they disrupt the normally smooth cyclotron motion of the protons, leading to non-conservation of the first adiabatic invariant, the magnetic moment (McChesney, Stern & Bellan 1987; Chen, Lin & White 2001*a*; Johnson & Cheng 2001; Chaston *et al.* 2004*a*; Fiksel *et al.* 2009; Xia *et al.* 2013). Chandran *et al.* (2010) used phenomenological arguments to derive an analytical formula for the stochastic-heating rate at $\beta_\mathrm{p} \lesssim 1$, where β_p is the ratio of the proton pressure

[1] We neglect the mass density of electrons and heavy ions.

to the magnetic pressure (see (2.3)). In § 2 we use phenomenological arguments to obtain an analytic formula for the proton-stochastic-heating rate in low-frequency AW/KAW turbulence when $\beta_\mathrm{p} \sim 1$–30. We limit our analysis to $\beta_\mathrm{p} \lesssim 30$, since KAWs become non-propagating at $k_\perp \rho_\mathrm{th} = 1$ at larger β_p values (see appendix A and Hellinger & Matsumoto (2000), Kawazura *et al.* (2018), Kunz *et al.* (2018)). In § 3 we present results from simulations of test particles interacting with a spectrum of randomly phased AWs/KAWs, which we use to test our analytic formula for the stochastic-heating rate. Throughout this paper, we focus on perpendicular proton heating rather than parallel proton heating. Stochastic heating can in principle to the parallel proton heating that results from linear damping of AW/KAW turbulence at $\beta_{\parallel\mathrm{p}} \gtrsim 1$, but we leave a discussion of this possibility to future work.

2. Stochastic proton heating by AW/KAW turbulence at the proton gyroscale

A proton interacting with a uniform background magnetic field $\boldsymbol{B}_0$ and fluctuating electric and magnetic fields $\delta\boldsymbol{E}$ and $\delta\boldsymbol{B}$ undergoes nearly periodic motion in the plane perpendicular to $\boldsymbol{B}_0$ if δE and δB are sufficiently small or L/ρ is sufficiently large, where L is the characteristic length scale of $\delta\boldsymbol{E}$ and $\delta\boldsymbol{B}$, $\rho = v_\perp/\Omega$ is the proton's gyroradius, $\boldsymbol{v}_\perp$ is the component of the proton's velocity $\boldsymbol{v}$ perpendicular to the magnetic field, $\Omega = qB_0/mc$ is the proton gyrofrequency, m and q are the proton mass and charge and c is the speed of light. When (i) the proton's motion in the plane perpendicular to $\boldsymbol{B}_0$ is nearly periodic and (ii) $\Omega\tau \gg 1$, where τ is the characteristic time scale of $\delta\boldsymbol{E}$ and $\delta\boldsymbol{B}$, the proton's magnetic moment $\mu = mv_\perp^2/2B_0$ is almost exactly conserved (Kruskal 1962).

Perpendicular heating of protons (by which we mean a secular increase in the average value of μ) requires that one of the above two conditions for μ conservation be violated. For example, Alfvén/ion-cyclotron waves can cause perpendicular proton heating via a cyclotron resonance if $\Omega\tau \sim 1$ (Hollweg & Isenberg 2002). Alternatively, low-frequency AW/KAW fluctuations can cause perpendicular proton heating if their amplitudes at $k_\perp\rho \sim 1$ are sufficiently large that the proton motion in the plane perpendicular to $\boldsymbol{B}_0$ becomes disordered or 'stochastic' (McChesney *et al.* 1987; Johnson & Cheng 2001; Chen, Lin & White 2001*b*; Chaston *et al.* 2004*b*; Fiksel *et al.* 2009).

We focus on this second type of heating, stochastic heating, and on 'thermal' protons, for which

$$v_\parallel \sim w_\parallel \quad v_\perp \sim w_\perp \quad \rho \sim \rho_\mathrm{th}, \tag{2.1a–c}$$

where $w_\perp = \sqrt{2k_\mathrm{B}T_{\perp\mathrm{p}}/m}$ and $w_\parallel = \sqrt{2k_\mathrm{B}T_{\parallel\mathrm{p}}/m}$ are the perpendicular and parallel thermal speeds, $T_{\perp\mathrm{p}}$ and $T_{\parallel\mathrm{p}}$ are the perpendicular and parallel proton temperatures, k_B is Boltzmann's constant and $\rho_\mathrm{th} = w_\perp/\Omega$ is the thermal-proton gyroradius. We restrict our attention to the contribution to the stochastic-heating rate from turbulent AW/KAW fluctuations with

$$\lambda \sim \rho_\mathrm{th} \quad k_\perp\rho_\mathrm{th} \sim 1, \tag{2.2a,b}$$

where λ is the length scale of the fluctuations measured perpendicular to the background magnetic field, and to

$$\beta_\mathrm{p} \equiv \frac{8\pi n k_\mathrm{B} T_\mathrm{p}}{B_0^2} \sim 1\text{–}30, \tag{2.3}$$

where

$$T_\mathrm{p} = \frac{2T_{\perp\mathrm{p}} + T_{\parallel\mathrm{p}}}{3}. \tag{2.4}$$

As mentioned above and discussed further in appendix A, KAWs at $k_\perp \rho_{\rm th} = 1$ become non-propagating at significantly larger values of $\beta_{\rm p}$ (see also Hellinger & Matsumoto 2000; Kawazura *et al.* 2018; Kunz *et al.* 2018). For simplicity, we assume that

$$T_{\perp {\rm p}} \sim T_{\parallel {\rm p}} \quad w_\perp \sim w_\parallel, \tag{2.5a,b}$$

which implies that

$$\beta_{\rm p} \sim \frac{w_\perp^2}{v_{\rm A}^2} \sim \frac{w_\parallel^2}{v_{\rm A}^2}, \tag{2.6}$$

and that $T_{\rm e} \sim T_{\rm p}$, where $T_{\rm e}$ is the electron temperature. We also assume that

$$\delta B_\rho \ll B_0, \tag{2.7}$$

where δB_ρ is the root-mean-square (r.m.s.) amplitude of the magnetic fluctuations with $\lambda \sim \rho_{\rm th}$, and that the fluctuations are in critical balance (Goldreich & Sridhar 1995), which implies that

$$\frac{\delta v_\rho}{\rho_{\rm th}} \sim \frac{v_{\rm A}}{l}, \tag{2.8}$$

where l is the correlation length of the gyroscale AW/KAW fluctuations measured parallel to the background magnetic field, and δv_ρ is the r.m.s. amplitude of the $\boldsymbol{E} \times \boldsymbol{B}$ velocity of the AW/KAW fluctuations with $\lambda \sim \rho_{\rm th}$. Since the linear and nonlinear time scales are comparable in the critical-balance model, we take the ratios of the amplitudes of different fluctuating variables to be comparable to the ratios that arise for linear AW/KAWs at $k_\perp \rho_{\rm th} \sim 1$, which, given (2.2) and (2.3), implies that

$$\delta B_{\parallel \rho} \sim \delta B_{\perp \rho} \sim \delta B_\rho \quad \frac{\delta B_\rho}{B_0} \sim \frac{\delta v_\rho}{v_{\rm A}}, \tag{2.9a,b}$$

where $\delta B_{\parallel \rho}$ and $\delta B_{\perp \rho}$ are, respectively, the r.m.s. amplitudes of the components of the fluctuating magnetic field parallel and perpendicular to $\boldsymbol{B}_0$ (TenBarge *et al.* 2012). Equations (2.2) through (2.9) imply that

$$\omega \sim \frac{v_{\rm A}}{l} \sim \frac{\delta v_\rho}{\rho_{\rm th}} \sim \Omega \frac{\delta v_\rho}{w_\perp} \sim \Omega \beta_{\rm p}^{-1/2} \frac{\delta v_\rho}{v_{\rm A}} \sim \Omega \beta_{\rm p}^{-1/2} \frac{\delta B_\rho}{B_0} \ll \Omega. \tag{2.10}$$

2.1. *Stochastic motion perpendicular to the magnetic field*

To understand how gyroscale AW/KAW fluctuations modify a proton's motion, we cannot use the adiabatic approximation (Northrop 1963), which assumes $\lambda \gg \rho$. Nevertheless, we can still define an effective guiding centre

$$\boldsymbol{R} = \boldsymbol{r} + \frac{\boldsymbol{v} \times \hat{\boldsymbol{b}}}{\Omega}, \tag{2.11}$$

where $\hat{\boldsymbol{b}} = \boldsymbol{B}/B$. This effective guiding centre is always a distance ρ from the particle's position $\boldsymbol{r}$ and is, at any given time, the location about which the particle attempts to gyrate under the influence of the Lorentz force. We find it useful to focus on $\boldsymbol{R}$ rather than $\boldsymbol{r}$ because the motion of $\boldsymbol{R}$ largely excludes the high-frequency cyclotron

motion of the proton. Upon taking the time derivative of (2.11) and making use of the relations $\mathrm{d}\boldsymbol{r}/\mathrm{d}t = \boldsymbol{v}$ and $\mathrm{d}\boldsymbol{v}/\mathrm{d}t = (q/m)(\boldsymbol{E} + \boldsymbol{v} \times \boldsymbol{B}/c)$, we obtain

$$\frac{\mathrm{d}\boldsymbol{R}}{\mathrm{d}t} = v_\parallel \hat{\boldsymbol{b}} + \frac{c\boldsymbol{E} \times \boldsymbol{B}}{B^2} - \frac{\boldsymbol{v} \times \hat{\boldsymbol{b}}}{\Omega} \frac{1}{B} \frac{\mathrm{d}B}{\mathrm{d}t} + \frac{\boldsymbol{v}}{\Omega} \times \frac{\mathrm{d}\hat{\boldsymbol{b}}}{\mathrm{d}t}, \tag{2.12}$$

where $v_\parallel = \boldsymbol{v} \cdot \hat{\boldsymbol{b}}$. The perpendicular component of $\mathrm{d}\boldsymbol{R}/\mathrm{d}t$,

$$\left(\frac{\mathrm{d}\boldsymbol{R}}{\mathrm{d}t}\right)_\perp = \frac{\mathrm{d}\boldsymbol{R}}{\mathrm{d}t} - \hat{\boldsymbol{b}} \left(\hat{\boldsymbol{b}} \cdot \frac{\mathrm{d}\boldsymbol{R}}{\mathrm{d}t}\right) = \left(\hat{\boldsymbol{b}} \times \frac{\mathrm{d}\boldsymbol{R}}{\mathrm{d}t}\right) \times \hat{\boldsymbol{b}}, \tag{2.13}$$

can be found by substituting the right-hand side of (2.12) into the right-hand side of (2.13), which yields

$$\left(\frac{\mathrm{d}\boldsymbol{R}}{\mathrm{d}t}\right)_\perp = \frac{c\boldsymbol{E} \times \boldsymbol{B}}{B^2} - \frac{\boldsymbol{v} \times \hat{\boldsymbol{b}}}{\Omega} \frac{1}{B} \frac{\mathrm{d}B}{\mathrm{d}t} + \frac{v_\parallel}{\Omega} \hat{\boldsymbol{b}} \times \frac{\mathrm{d}\hat{\boldsymbol{b}}}{\mathrm{d}t}. \tag{2.14}$$

We now estimate each term on the right-hand side of (2.14). Since we are considering only gyroscale fluctuations,[2] the first term on the right-hand side of (2.14) satisfies the relation

$$\left|\frac{c\boldsymbol{E} \times \boldsymbol{B}}{B^2}\right| \sim \delta v_\rho. \tag{2.15}$$

To estimate the second and third terms on the right-hand side of (2.14), we take

$$v_\perp \sim |v_\parallel| \sim w_\perp \sim w_\parallel, \tag{2.16}$$

which is satisfied by the majority of particles. The time derivative of the field strength along the particle's trajectory is

$$\frac{\mathrm{d}B}{\mathrm{d}t} = \frac{\partial B}{\partial t} + \boldsymbol{v}_\perp \cdot \boldsymbol{\nabla} B + v_\parallel \hat{\boldsymbol{b}} \cdot \boldsymbol{\nabla} B. \tag{2.17}$$

As outlined above, our assumption of critical balance implies that $\lambda \ll l$ and $\omega \ll v_\perp/\rho \sim w_\perp/\rho_{\mathrm{th}}$. The second term on the right-hand side of (2.17) is thus much larger than either the first or third terms, and

$$\frac{\mathrm{d}B}{\mathrm{d}t} \sim \frac{w_\perp \delta B_{\parallel\rho}}{\rho_{\mathrm{th}}}. \tag{2.18}$$

The second term on the right-hand side of (2.14) thus satisfies

$$\left|\frac{\boldsymbol{v} \times \hat{\boldsymbol{b}}}{\Omega} \frac{1}{B} \frac{\mathrm{d}B}{\mathrm{d}t}\right| \sim \frac{\rho_{\mathrm{th}}}{B} \frac{\mathrm{d}B}{\mathrm{d}t} \sim \frac{w_\perp \delta B_{\parallel\rho}}{B_0}, \tag{2.19}$$

which is larger than the first term on the right-hand side of (2.14) by a factor of $\sim \beta_{\mathrm{p}}^{1/2}$, given (2.6) and (2.9).

[2] AW fluctuations at $\lambda \gg \rho_{\mathrm{th}}$ advect both the gyroscale AW/KAW eddies and the particles at the $\boldsymbol{E} \times \boldsymbol{B}$ velocity of the large-scale AW fluctuations.

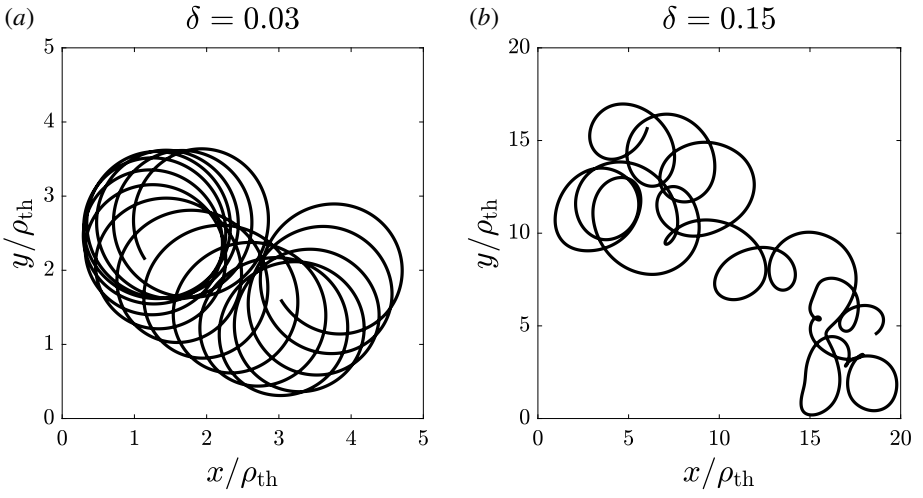

FIGURE 1. Trajectories of test-particle protons interacting with a spectrum of randomly phased AWs and KAWs for different values of the stochasticity parameter δ defined in (2.21).

For the moment, we assume that the second term on the right-hand side of (2.14) is the dominant term; we discuss the third term in more detail below. If the second term is dominant, then

$$\left|\left(\frac{\mathrm{d}\boldsymbol{R}}{\mathrm{d}t}\right)_{\perp}\right| \sim \frac{w_{\perp}\delta B_{\parallel\rho}}{B_0}. \tag{2.20}$$

During a single cyclotron period $2\pi/\Omega$, a proton passes through an order-unity number of uncorrelated gyroscale AW/KAW eddies, and the values of $(\mathrm{d}\boldsymbol{R}/\mathrm{d}t)_{\perp}$ within different gyroscale eddies are uncorrelated. If $(\mathrm{d}\boldsymbol{R}/\mathrm{d}t)_{\perp}$ is small compared to $w_{\perp}$, then a proton undergoes nearly circular gyromotion. However, if $|(\mathrm{d}\boldsymbol{R}/\mathrm{d}t)_{\perp}|$ is a significant fraction of $w_{\perp}$, then a proton and its guiding centre will move in an essentially unpredictable way, and the proton's orbit will become stochastic rather than quasi-periodic. Given (2.9), $|(\mathrm{d}\boldsymbol{R}/\mathrm{d}t)_{\perp}|$ is a significant fraction of $w_{\perp}$ if the stochasticity parameter

$$\delta \equiv \frac{\delta B_{\rho}}{B_0} \tag{2.21}$$

is a significant fraction of unity.

We illustrate how the value of δ affects a proton's motion in figure 1. We compute the particle trajectories shown in this figure by numerically integrating the equations of motion for protons interacting with randomly phased AWs and KAWs. We present the details of our numerical method and more extensive numerical results in § 3. In the numerical calculation shown in figure 1(*a*), $\delta = 0.03$, and the proton's motion in the plane perpendicular to $\boldsymbol{B}_0$ is quasi-periodic. In the numerical calculation shown in figure 1(*b*), $\delta = 0.15$, and the proton trajectory is more disordered or random.

We now consider the third term on the right-hand side of (2.14). The instantaneous value of this term is comparable to the instantaneous value of the second term given (2.9) and (2.16), but the third term is less effective at causing guiding-centre displacements over time for the following reason. Because of (2.7), the time $t_{\parallel}$ required for $v_{\parallel}$ to change by a factor of order unity is $\gg \Omega^{-1}$. If we integrate the

third term on the right-hand side of (2.14) from $t=0$ to $t=t_{\rm f}$, where $\Omega^{-1} \ll t_{\rm f} \ll t_{\parallel}$, we can treat $v_{\parallel}$ as approximately constant in (2.14), obtaining

$$\int_0^{t_{\rm f}} \frac{v_{\parallel}}{\Omega}\hat{\boldsymbol{b}} \times \frac{{\rm d}\hat{\boldsymbol{b}}}{{\rm d}t}\,{\rm d}t = \frac{v_{\parallel}}{\Omega_0}\frac{\boldsymbol{B}_0}{B_0} \times \Delta\hat{\boldsymbol{b}} \tag{2.22}$$

to leading order in $\delta B_\rho/B_0$, where $\Omega_0 = qB_0/mc$ and $\Delta\hat{\boldsymbol{b}} = \hat{\boldsymbol{b}}(t_{\rm f}) - \hat{\boldsymbol{b}}(0)$ is the change in $\hat{\boldsymbol{b}}$. There is, however, no secular change in the value of $\hat{\boldsymbol{b}}$ at the proton's location; the magnetic-field unit vector merely undergoes small-amplitude fluctuations about the direction of the background magnetic field. Thus, over time, the guiding-centre displacements caused by the third term on the right-hand side of (2.14) are largely reversible and tend to cancel out. The third term is thus less effective than the second term at making proton orbits stochastic.

When the stochasticity parameter δ defined in (2.21) exceeds some threshold, the motion of a thermal proton's guiding centre in the plane perpendicular to $\boldsymbol{B}_0$ is reasonably approximated by a random walk. To estimate the time step of this random walk, we begin by defining the cyclotron average of $({\rm d}\boldsymbol{R}/{\rm d}t)_\perp$,

$$\boldsymbol{v}_R(t) \equiv \frac{\Omega}{2\pi}\int_{t-\pi/\Omega}^{t+\pi/\Omega}\left(\frac{{\rm d}\boldsymbol{R}}{{\rm d}t_1}\right)_\perp {\rm d}t_1. \tag{2.23}$$

As stated above, during a single cyclotron period, a proton's motion projected onto the plane perpendicular to $\boldsymbol{B}_0$ carries the proton through an order-unity number of uncorrelated gyroscale AW/KAW 'eddies'. For simplicity, we take the amplitude and direction of each vector term on the right-hand side of (2.14) to be approximately constant within any single gyroscale eddy and the values of these vector terms within different eddies to be uncorrelated. This makes $\boldsymbol{v}_R$ approximately equal to the average of some order-unity number of uncorrelated vectors of comparable magnitude. The amplitude of this average is comparable to the instantaneous value of $|({\rm d}\boldsymbol{R}/{\rm d}t)_\perp|$. Thus, given (2.6), (2.9), and (2.20),

$$v_R \sim \frac{w_\perp \delta B_{\parallel\rho}}{B_0} \sim \beta_{\rm p}^{1/2}\delta v_\rho. \tag{2.24}$$

Because we are considering the effects of just the gyroscale AW/KAW eddies, $\boldsymbol{v}_R$ decorrelates after the proton's guiding centre has moved a distance $\sim\rho_{\rm th}$ in the plane perpendicular to $\boldsymbol{B}_0$, which takes a time

$$\Delta t \sim \frac{\rho_{\rm th}}{v_R}. \tag{2.25}$$

Thermal protons thus undergo spatial diffusion in the plane perpendicular to $\boldsymbol{B}_0$ with a spatial diffusion coefficient

$$D_\perp \sim \frac{\rho_{\rm th}^2}{\Delta t} \sim \beta_{\rm p}^{1/2}\delta v_\rho \rho_{\rm th}. \tag{2.26}$$

Given (2.8), (2.16) and (2.24),

$$\Delta t \sim \frac{\rho_{\rm th}}{\beta_{\rm p}^{1/2}\delta v_\rho} \sim \frac{l}{\beta_{\rm p}^{1/2} v_{\rm A}} \sim \frac{l}{v_\parallel}. \tag{2.27}$$

The time required for a particle to wander a distance $\sim\rho_{\rm th}$ perpendicular to the background magnetic field is thus comparable to the time required for the particle to traverse the parallel dimension of a gyroscale AW/KAW eddy.

2.2. *Energy diffusion and heating*

The total energy of a proton is given by its Hamiltonian,

$$H = q\Phi + \frac{1}{2m}\left(\boldsymbol{p} - \frac{q}{c}\boldsymbol{A}\right)^2, \tag{2.28}$$

where Φ is the electrostatic potential, $\boldsymbol{p}$ is the canonical momentum and $\boldsymbol{A}$ is the vector potential. From Hamilton's equations,

$$\frac{\mathrm{d}H}{\mathrm{d}t} = q\frac{\partial \Phi}{\partial t} - \frac{q\boldsymbol{v}}{c}\cdot\frac{\partial \boldsymbol{A}}{\partial t}, \tag{2.29}$$

where $\boldsymbol{v} = m^{-1}(\boldsymbol{p} - q\boldsymbol{A}/c)$ is the velocity, and the electric field is $\boldsymbol{E} = -\boldsymbol{\nabla}\Phi - c^{-1}\partial \boldsymbol{A}/\partial t$. The second term on the right-hand side of (2.29) is $q\boldsymbol{v}\cdot\boldsymbol{E}_\mathrm{s}$, where $\boldsymbol{E}_\mathrm{s} = -c^{-1}\partial \boldsymbol{A}/\partial t$ is the solenoidal component of the electric field. Equation (46) of Hollweg (1999) gives the ratio of E_s to the magnitude of the irrotational component of the electric field $|\boldsymbol{\nabla}\Phi|$ for AWs/KAWs with $k_\perp \rho_\mathrm{th} \lesssim 1$,[3]

$$\frac{E_\mathrm{s}}{|\boldsymbol{\nabla}\Phi|} \sim \frac{\beta_\mathrm{p}\omega}{\Omega}. \tag{2.30}$$

In their treatment of stochastic heating at $\beta_\mathrm{p} \lesssim 1$, Chandran *et al.* (2010) neglected the second term on the right-hand side of (2.29), because this term makes a small contribution to the heating rate when β_p is small. Here we focus on the effects of $\boldsymbol{E}_\mathrm{s}$ and make the approximation that

$$\frac{\mathrm{d}H}{\mathrm{d}t} \sim q\boldsymbol{v}\cdot\boldsymbol{E}_\mathrm{s}. \tag{2.31}$$

We show in appendix B that the irrotational part of the electric field contributes less to the heating rate than does the solenoidal part when $\beta_\mathrm{p} \gtrsim 1$.

As a proton undergoes spatial diffusion in the plane perpendicular to the background magnetic field, the electromagnetic field at its location resulting from gyroscale AW/KAW fluctuations decorrelates on the time scale Δt given in (2.27). Within each time interval of length $\sim\Delta t$, the proton energy changes by an amount δH (which can be positive or negative), and the values of δH are uncorrelated within successive time intervals of length Δt. As a consequence, the proton undergoes energy diffusion.

To estimate the r.m.s. value of δH, which we denote ΔH, we adopt a simple model of a proton's motion, in which the proton's complicated trajectory is replaced by a repeating two-step process. In the first step, the proton undergoes circular cyclotron motion in the plane perpendicular to $\boldsymbol{B}_0$ for a time Δt. In the second step, the proton is instantly translated a distance ρ_th in some random direction perpendicular to $\boldsymbol{B}_0$.[4]

In this simple model, a proton undergoes $N \sim \Omega\Delta t \sim (v_\perp/\rho_\mathrm{th}) \times (l/v_\parallel) \sim l/\rho_\mathrm{th} \gg 1$ circular gyrations in the plane perpendicular to $\boldsymbol{B}_0$ during a time Δt. Integrating (2.31) for a time Δt, we obtain

$$\delta H \sim q\int_0^{\Delta t} \boldsymbol{v}(t)\cdot\boldsymbol{E}_\mathrm{s}(\boldsymbol{r}(t), t)\,\mathrm{d}t, \tag{2.32}$$

[3] $\boldsymbol{E}_\mathrm{s}$ is nearly perpendicular to $\boldsymbol{B}_0$, as illustrated in figure 3 of Hollweg (1999).

[4] For simplicity, our model of proton motion neglects motion parallel to $\boldsymbol{B}$. This approximation is to some extent justified by (2.27), which implies that a proton is unable to escape from an eddy of length l by motion along the magnetic field in a time shorter than Δt. However, we return to the issue of parallel motion in § 2.3.

where $\boldsymbol{r}(t)$ is the proton's position at time t. Since $\Delta t \sim \beta_{\mathrm{p}}^{-1/2}\rho_{\mathrm{th}}/\delta v_{\rho}$, when $\beta_{\mathrm{p}} \gtrsim 1$, the time Δt for a particle to diffuse across one set of gyroscale eddies is shorter than or comparable to the linear or nonlinear time scale $\rho_{\mathrm{th}}/\delta v_{\rho}$ of those eddies. We thus approximate the right-hand side of (2.32) by setting $\boldsymbol{E}_{\mathrm{s}}(\boldsymbol{r}(t), t) = \boldsymbol{E}_{\mathrm{s}}(\boldsymbol{r}(t), 0)$ and rewrite (2.32) as

$$\delta H \sim qN \oint \boldsymbol{E}_{\mathrm{s}}(\boldsymbol{r}, 0) \cdot \mathrm{d}\boldsymbol{l} \sim qN \int_S \boldsymbol{\nabla} \times \boldsymbol{E}(\boldsymbol{r}, 0) \cdot \mathrm{d}\boldsymbol{S} \sim -\frac{qN}{c} \int_S \frac{\partial \boldsymbol{B}}{\partial t}(\boldsymbol{r}, 0) \cdot \mathrm{d}\boldsymbol{S}, \tag{2.33}$$

where the line integral is along the proton's path during one complete circular gyration in the plane perpendicular to $\boldsymbol{B}_0$, the surface integral is over the circular surface S of radius ρ_{th} enclosed by the gyration, and we have used Faraday's law $\boldsymbol{\nabla} \times \boldsymbol{E} = (-1/c)\partial \boldsymbol{B}/\partial t$. The surface S is perpendicular to $\boldsymbol{B}_0$, and $\mathrm{d}\boldsymbol{S}$ is anti-parallel to $\boldsymbol{B}_0$ (anti-parallel rather than parallel since $q > 0$). The r.m.s. value of δH thus satisfies the order-of-magnitude relation

$$\Delta H \sim \frac{qN}{c} \omega_{\mathrm{eff}} \delta B_{\parallel\rho} \rho_{\mathrm{th}}^2, \tag{2.34}$$

where

$$\omega_{\mathrm{eff}} \equiv \frac{\delta v_{\rho}}{\rho_{\mathrm{th}}} \tag{2.35}$$

is the nonlinear frequency of the gyroscale fluctuations. Upon setting $q/c = \Omega m/B$, $N = \Omega \Delta t$ and $\rho_{\mathrm{th}}^2 = w_{\perp}^2/\Omega^2$ in (2.34), we obtain

$$\Delta H \sim \frac{m w_{\perp}^2}{B} \frac{\delta v_{\rho}}{\rho_{\mathrm{th}}} \delta B_{\parallel\rho} \Delta t. \tag{2.36}$$

Although we are in the process of estimating the rate at which μ changes over long times, our estimate of ΔH is comparable to the value that would follow from μ conservation: $\Delta H \sim \mu \Delta B \sim (m w_{\perp}^2/B)\omega_{\mathrm{eff}} \delta B_{\parallel\rho} \Delta t$, where $\Delta B \sim \omega_{\mathrm{eff}} \delta B_{\parallel\rho} \Delta t$ is the r.m.s. amplitude of the change in the magnetic flux through the proton's Larmor orbit, divided by $\pi\rho^2$, during the time Δt in which the proton is (in our simple two-step model of proton motion) undergoing continuous, circular, cyclotron motion. This correspondence highlights an alternative interpretation of the stochastic-heating process at $\beta_{\mathrm{p}} \gtrsim 1$. In the guiding-centre approximation, when $v_{\perp}^2$ increases by some factor because of $\boldsymbol{E}_{\mathrm{s}}$, the field strength at the particle's guiding centre increases by approximately the same factor, essentially because of Faraday's law. This proportionality underlies μ conservation. In stochastic heating, the same proportionality is approximately satisfied during a single time interval Δt, but the proton is then stochastically transported to a neighbouring set of gyroscale eddies, in which the field strength is not correlated with the field strength at the proton's original location. The proton thus 'forgets' about what happened to the field strength at its original location and gets to keep the energy that it gained without 'paying the price' of residing in a higher-field-strength location. In this way, spatial diffusion perpendicular to $\boldsymbol{B}$ breaks the connection between changes to $v_{\perp}^2$ and changes to B that arises in the $\rho/\lambda \to 0$ limit.

In our simple model, the energy gained by a proton is in the form of perpendicular kinetic energy,

$$K_{\perp} = \frac{m v_{\perp}^2}{2}, \tag{2.37}$$

because we neglect the parallel motion of protons. (We do not preclude the possibility of parallel stochastic heating, but we do not consider it further here.) The perpendicular-kinetic-energy diffusion coefficient D_K is thus $\sim\Delta H^2/\Delta t$, or

$$D_K \sim \frac{m^2 w_\perp^4}{\beta_\mathrm{p}^{1/2}} \frac{\delta v_\rho}{\rho_\mathrm{th}} \frac{\delta B_\rho^2}{B_0^2}, \tag{2.38}$$

where we have used (2.27) to estimate Δt and (2.9) to set $\delta B_{\parallel\rho} \sim \delta B_\rho$. A single proton undergoing a random walk in energy can gain or lose energy with equal probability during a time Δt. However, if a large number of thermal protons (e.g. with an initially Maxwellian distribution) undergo energy diffusion, then on average more protons will gain energy than lose energy, leading to proton heating. The heating time scale τ_h is the characteristic time for the perpendicular kinetic energy of a thermal proton to double, $\tau_\mathrm{h} \sim (m w_\perp^2)^2/D_K$, and the perpendicular-heating rate per unit mass is $Q_\perp \sim K_\perp/(m\tau_\mathrm{h}) \sim D_K/(mK_\perp)$, or,

$$Q_\perp \sim \beta_\mathrm{p}^{1/2} \frac{(\delta v_\rho)^3}{\rho_\mathrm{th}}. \tag{2.39}$$

To account for the uncertainties introduced by our numerous order-of-magnitude estimates, we multiply the right-hand side of (2.39) by an as-yet-unknown dimensionless constant σ_1. As $\delta v_\rho \to 0$, $\mathrm{d}\mu/\mathrm{d}t$ decreases faster than any power of δv_ρ (Kruskal 1962). To account for this 'exponential' μ conservation in the small-δv_ρ limit, we follow Chandran *et al.* (2010) by multiplying the right-hand side of (2.39) by the factor $\exp(-\sigma_2/\delta)$,

$$Q_\perp = \sigma_1 \frac{(\delta v_\rho)^3}{\rho_\mathrm{th}} \sqrt{\beta_\mathrm{p}} \exp\left(-\frac{\sigma_2}{\delta}\right), \tag{2.40}$$

where σ_2 is another as-yet-unknown dimensionless constant, and δ is defined in (2.21).

For comparison, the stochastic-heating rate per unit mass found by Chandran *et al.* (2010) when $\beta_\mathrm{p} \lesssim 1$ is

$$Q_\perp = c_1 \frac{(\delta v_\rho)^3}{\rho_\mathrm{th}} \exp\left(-\frac{c_2}{\varepsilon}\right), \tag{2.41}$$

where

$$\varepsilon = \frac{\delta v_\rho}{w_\perp}, \tag{2.42}$$

and the dimensionless constants c_1 and c_2 serve the same purpose as those in (2.40). As discussed by Chandran *et al.* (2010) for the case of c_1 and c_2, we expect the constants σ_1 and σ_2 to depend on the nature of the fluctuations. For example, at fixed δv_ρ, we expect stronger heating rates (i.e. larger σ_1 and/or smaller σ_2) from intermittent turbulence than from randomly phased waves (Chandran *et al.* 2010; Xia *et al.* 2013; Mallet *et al.* 2018), because, in intermittent turbulence, most of the heating takes place near coherent structures in which the fluctuations are unusually strong and in which the proton orbits are more stochastic than on average.

2.3. *Orbit stochasticity from parallel motion*

In § 2.1, we focused on proton motion perpendicular to $\boldsymbol{B}$. However, motion along the magnetic field can also produce stochastic motion in the plane perpendicular to $\boldsymbol{B}_0$ (see, e.g. Hauff *et al.* 2010). In particular, the perpendicular magnetic fluctuations at

the scale of a proton's gyroradius perturb the direction of $\hat{\boldsymbol{b}}$. These perturbations, when fed into the first term on the right-hand side of (2.12), $v_\parallel \hat{\boldsymbol{b}}$, cause the proton's guiding centre $\boldsymbol{R}$ to acquire a velocity perpendicular to $\boldsymbol{B}_0$ of

$$\boldsymbol{u}_\perp \sim v_\parallel \times \frac{\delta \boldsymbol{B}_{\perp\rho}}{B_0}, \tag{2.43}$$

where $\delta \boldsymbol{B}_{\perp\rho}$ is the component of $\delta \boldsymbol{B}$ (from gyroscale fluctuations) perpendicular to $\boldsymbol{B}_0$ at the proton's location. The value of $\boldsymbol{u}_\perp$ varies in an incoherent manner in time, with a correlation time $\sim \Omega^{-1}$. If $u_\perp$ is a significant fraction of $v_\perp$, then $\boldsymbol{u}_\perp$ will cause a proton's orbit in the plane perpendicular to $\boldsymbol{B}_0$ to become stochastic. This leads to an alternative high-$\beta_{\rm p}$ stochasticity parameter,

$$\tilde{\delta} = \frac{u_\perp}{v_\perp} = \frac{v_\parallel \delta B_{\perp\rho}}{v_\perp B_0}. \tag{2.44}$$

As $\tilde{\delta}$ increases towards unity, proton orbits become stochastic. For thermal protons with $v_\perp \sim v_\parallel$ and $\rho \sim \rho_{\rm th}$, $\tilde{\delta}$ is equivalent to δ in (2.21), which was based upon the parallel magnetic-field fluctuation $\delta B_{\parallel\rho}$ (even though we set $\delta B_{\parallel\rho} \sim \delta B_\rho$ in (2.21))). The contribution of parallel motion to orbit stochasticity thus does not change our conclusions about the rate at which thermal protons are heated stochastically. However, the contribution of parallel motion to orbit stochasticity should be taken into account when considering the ability of stochastic heating to produce superthermal tails, because in AW turbulence the perpendicular (parallel) magnetic fluctuation at perpendicular scale λ, denoted $\delta B_{\perp\lambda}$ ($\delta B_{\parallel\lambda}$), is an increasing (decreasing) function of λ when λ is in the inertial range. Orbit stochasticity through the interaction between parallel motion and $\delta B_{\perp\rho}$ could thus contribute to the development of superthermal tails when $\beta_{\rm p} \gtrsim 1$. An investigation of superthermal tails, however, lies beyond the scope of this paper.

3. Numerical test-particle calculations

To test the phenomenological theory developed in § 2, we numerically track test-particle protons interacting with a spectrum of low-frequency randomly phased AWs and KAWs. The initial particle positions are random and uniformly distributed within a cubical region of volume $(100 d_{\rm p})^3$, where $d_{\rm p} = v_{\rm A}/\Omega$ is the proton inertial length. The initial velocity distribution is an isotropic Maxwellian with proton temperature $T_{\rm p}$. To trace each particle, we solve the equations of motion,

$$\frac{{\rm d}\boldsymbol{x}}{{\rm d}t} = \boldsymbol{v} \quad \frac{{\rm d}\boldsymbol{v}}{{\rm d}t} = \frac{q}{m}\left(\boldsymbol{E} + \frac{\boldsymbol{v}\times\boldsymbol{B}}{c}\right), \tag{3.1}$$

using the Boris method (Boris 1970) with a time step of $0.01\Omega^{-1}$.

3.1. *Randomly phased waves*

The code used to implement the AW/KAW spectrum is similar to the code used by Chandran *et al.* (2010). The magnetic field is $\boldsymbol{B} = B_0\hat{\boldsymbol{z}} + \delta\boldsymbol{B}$, where B_0 is constant. We take $\boldsymbol{E}$ and $\delta\boldsymbol{B}$ to be the sum of the electric and magnetic fields of waves at each of 81 different wave vectors, with two waves of equal amplitude at each wave vector,

one with $\omega/k_z < 0$ and the other with $\omega/k_z > 0$.[5] The initial phase of each wave is randomly chosen.

The 81 wave vectors correspond to nine evenly spaced values of the azimuthal angle in $\boldsymbol{k}$ space (in cylindrical coordinates aligned with $\boldsymbol{B}_0$) at each of nine specific values of $k_{\perp i} : i \in [0, \ldots, 8]$. The values of $k_{\perp i}$ are evenly spaced in $\ln(k_\perp)$-space, with $\ln(k_{\perp i}\rho_{\rm th}) = -4/3 + i/3$. The middle three cells, in which $i = 3$, 4 and 5, have a combined width of unity in $\ln(k_\perp)$-space, centred at precisely $k_\perp \rho_{\rm th} = 1$. We computationally evaluate δv_ρ and δB_ρ via the r.m.s. values of the $\boldsymbol{E} \times \boldsymbol{B}$ velocity and $\delta \boldsymbol{B}$ that result from the waves in just these middle three cells.

There is one value of $k_\parallel \equiv |k_z|$ at each $k_{\perp i}$, denoted $k_{\parallel i}$. We determine $k_{\parallel 4}$ by setting the linear frequency at $k_{\parallel 4}$ equal to $k_{\perp 4}\delta v_\rho$. At other values of $k_\perp$, we set

$$\frac{k_{\parallel i}}{k_{\parallel 4}} = \begin{cases} \left(\dfrac{k_{\perp i}}{k_{\perp 4}}\right)^{2/3} & : 0 \leqslant i < 4 \\ \left(\dfrac{k_{\perp i}}{k_{\perp 4}}\right)^{1/3} & : 4 < i \leqslant 8. \end{cases} \tag{3.2}$$

The exponents 2/3 and 1/3 in (3.2) are chosen to match the scalings in the critical-balance models of Goldreich & Sridhar (1995) and Cho & Lazarian (2004), respectively. We take the individual wave magnetic-field amplitudes to be proportional to $k_\perp^{-1/3}$ and $k_\perp^{-2/3}$ for $k_\perp \rho_{\rm th} < 1$ and $k_\perp \rho_{\rm th} > 1$, respectively, in order to match the same two critical-balance models. (All the waves at the same value of $k_{\perp i}$ have the same amplitudes.) We determine the wave frequency and relative amplitudes of the different components of the fluctuating electric and magnetic fields using Hollweg's (1999) two-fluid analysis of linear KAWs, setting

$$\frac{T_{\rm e}}{T_{\rm p}} = 0.5 \quad \frac{v_{\rm A}}{c} = 0.003, \tag{3.3a,b}$$

where $T_{\rm e}$ and $T_{\rm p}$ are the (isotropic) electron and proton temperatures. We do not expect the particular choices in (3.3) to have a large effect on our results, but choose those values to facilitate a direct comparison to the previous numerical results of Chandran *et al.* (2010). Since we take $T_{\perp {\rm p}} = T_{\parallel {\rm p}}$, we set

$$w_\perp = w_\parallel = w \equiv \sqrt{\frac{2k_{\rm B}T_{\rm p}}{m}} = v_{\rm A}\sqrt{\beta_{\rm p}}. \tag{3.4}$$

3.2. *A note on the electric field*

Following Lehe *et al.* (2009), we correct the electric field because the magnetic field (including its fluctuations, i.e. $\boldsymbol{B} = B_0\hat{\boldsymbol{z}} + \delta\boldsymbol{B}$) in the simulation is not orientated along the z-axis. The simulation, however, equates the parallel and perpendicular components of the electric field to the parallel and perpendicular components of the wave electric field that would arise if the magnetic field were aligned exactly on the z-axis. The result is a numerical addition of perpendicular electric-field terms to the parallel electric field, which, in turn, causes non-physical parallel heating. This may be seen in figure 2 of Chandran *et al.* (2010). To fix this, we replace the sum of the individual wave electric fields described in § 3.1, which we denote $\boldsymbol{E}_{\rm wave}$, with the modified electric field $\boldsymbol{E} = \boldsymbol{E}_{\rm wave} + \hat{\boldsymbol{b}}(\hat{\boldsymbol{z}} \cdot \boldsymbol{E}_{\rm wave} - \hat{\boldsymbol{b}} \cdot \boldsymbol{E}_{\rm wave})$.

[5]This makes the cross-helicity zero. For a discussion of how cross-helicity affects the stochastic-heating rate in the low-$\beta_{\rm p}$ regime, see Chandran *et al.* (2013).

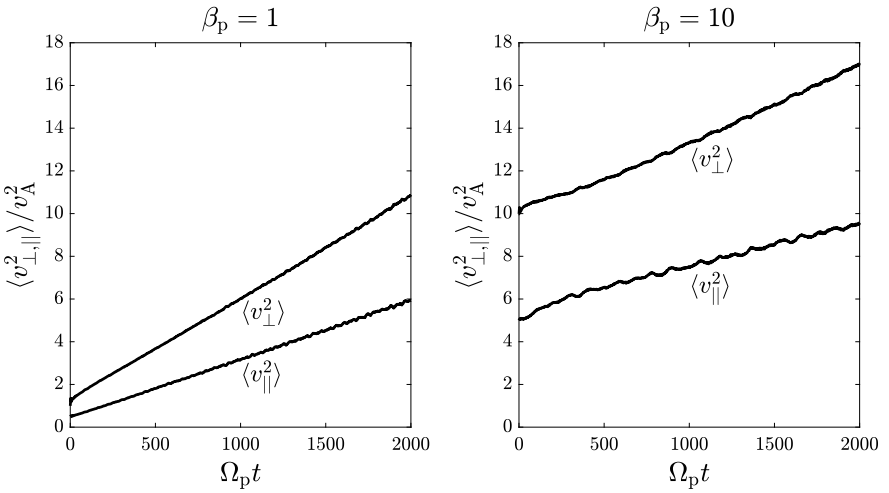

FIGURE 2. The mean square velocity perpendicular to $\boldsymbol{B}_0$, $\langle v_\perp^2\rangle$, as a function of time in two test-particle calculations, each of which tracks 10^5 protons. The value of the stochasticity parameter δ (defined in (2.21)) is 0.15 in both calculations.

3.3. *Perpendicular heating*

We perform numerical test-particle calculations at five different values of β_p, in particular $\beta_\mathrm{p} = \{0.006, 0.01, 0.1, 1, 10\}$. For each β_p value, we carry out test-particle calculations for five different values of δ (or, equivalently, five different values of ε). Each calculation returns the values of $\langle v_\perp^2\rangle$ and $\langle v_\parallel^2\rangle$ as functions of time. We show two examples in figure 2. The slope of the best-fit line for each $\langle v_\perp^2(t)\rangle$ curve determines the perpendicular-heating rate per unit mass $Q_\perp = (1/2)(\mathrm{d}/\mathrm{d}t)\langle v_\perp^2\rangle$, where $\langle\cdots\rangle$ indicates an average over the 10^4 or 10^5 particles in the simulation. (We use more particles in simulations with smaller ε and δ because the heating rates are smaller in these simulations, and the extra particles increase the signal-to-noise ratio.) We fit the $\langle v_\perp^2(t)\rangle$ curves during the time interval $(t_\mathrm{i}, t_\mathrm{f})$, where $t_\mathrm{i} = 20\pi/\Omega$ and t_f is the smaller of the following two values: $10^4\Omega^{-1}$ and the time required for $\langle v_\perp^2\rangle$ to increase by $\simeq 30\,\%$. We do not include the first ten cyclotron periods when calculating $Q_\perp$, because it takes the particles a few cyclotron periods to adjust to the presence of the waves, during which time there is typically strong transient heating. (As figure 2 shows, the test particles undergo parallel heating as well as perpendicular heating, as was found previously by Xia *et al.* (2013) in simulations of test particles interacting with reduced magnetohydrodynamic turbulence at $\beta_{\parallel\mathrm{p}} = 1$.)

The perpendicular-heating rates in our test-particle calculations are shown in figure 3. The solid-line curves in (*a*,*c*) on the left correspond to (2.41), with

$$c_1 = 0.77, \quad c_2 = 0.33. \tag{3.5a,b}$$

These values are very similar to the values $c_1 = 0.75$ and $c_2 = 0.34$ obtained by Chandran *et al.* (2010) at $\beta_\mathrm{p} = 0.006$. The solid-line curves in (*b*,*d*) on the right correspond to (2.40) with

$$\sigma_1 = 5.0, \quad \sigma_2 = 0.21. \tag{3.6a,b}$$

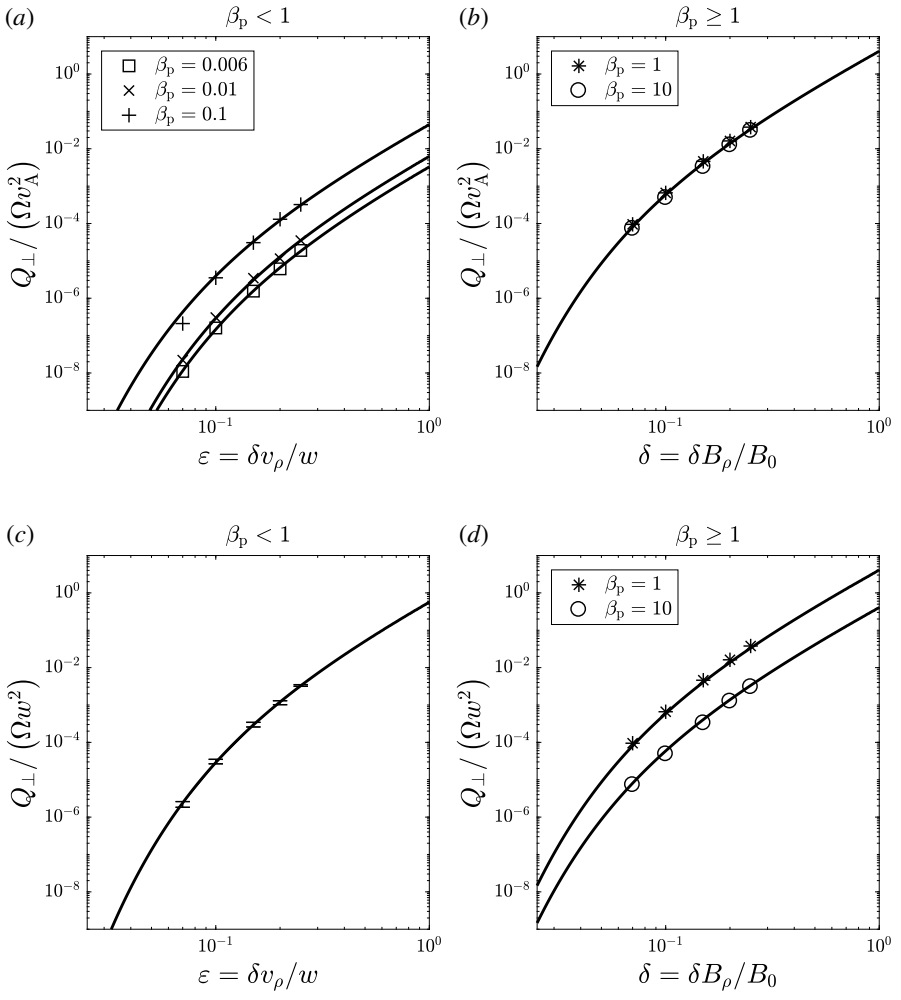

FIGURE 3. Numerical results for the perpendicular-heating rate per unit mass, $Q_\perp$, for protons interacting with randomly phased AWs and KAWs. (*a*) $\beta_p < 1$, and $Q_\perp$ normalized by Ωv_A^2. (*b*) $\beta_p \geqslant 1$ and $Q_\perp$ normalized by Ωv_A^2. (*c*) $\beta_p < 1$ and $Q_\perp$ normalized by Ωw^2, where w is the proton thermal speed defined in (3.4); the numerical results for all three β_p values (0.006, 0.01, and 0.1) are within the bars shown. (*d*) $\beta_p \geqslant 1$ and $Q_\perp$ normalized by Ωw^2. In (*a*,*c*) the solid lines are plots of (2.41) for the best-fit values of c_1 and c_2 given in (3.5). In (*b*,*d*) the solid lines are plots of (2.40) for the best-fit values of σ_1 and σ_2 in (3.6).

The agreement between our numerical results and (2.40) suggests that the approximations used to derive this equation are reasonable.

Figure 3(*c*) shows that at $\beta_p < 1$, $Q_\perp/(\Omega w^2)$ is a function of ε alone, consistent with the fact that (2.41) can be rewritten in the form

$$\frac{Q_\perp}{\Omega w^2} = c_1 \varepsilon^3 \exp\left(-\frac{c_2}{\varepsilon}\right) \quad (\text{at } \beta_p \lesssim 1). \tag{3.7}$$

Figure 3(*b*) shows that at $\beta_{\rm p} \geqslant 1$, $Q_\perp/(\Omega v_{\rm A}^2)$ is a function of δ alone, consistent with the fact that (2.40) can be rewritten as

$$\frac{Q_\perp}{\Omega v_{\rm A}^2} = \sigma_1 \delta^3 \exp\left(-\frac{\sigma_2}{\delta}\right) \quad (\text{at } \beta_{\rm p} \gtrsim 1). \tag{3.8}$$

We note that in our model of randomly phased KAWs (Chandran *et al.* 2010),

$$\frac{\delta B_\rho}{B_0} = 0.84 \frac{\delta v_\rho}{v_{\rm A}}, \tag{3.9}$$

and thus

$$\delta = \frac{\delta B_\rho}{B_0} = 0.84 \frac{\delta v_\rho}{v_{\rm A}} = 0.84 \beta_{\rm p}^{1/2} \frac{\delta v_\rho}{w_\perp} = 0.84 \beta_{\rm p}^{1/2} \varepsilon. \tag{3.10}$$

As a consequence, if we adopt the best-fit values of σ_1, σ_2, c_1 and c_2, then the value of $Q_\perp$ at $\beta_{\rm p} = 1$ in (2.40), which matches our test-particle calculations quite well, exceeds the value that would follow from (2.41) at $\beta_{\rm p} = 1$. A similar phenomenon was found by Xia *et al.* (2013) in numerical simulations of test particles interacting with strong reduced magnetohydrodynamic turbulence.

To obtain a fitting formula that can be used to model stochastic heating at large $\beta_{\rm p}$, small $\beta_{\rm p}$ and $\beta_{\rm p} \simeq 1$, we use (3.4) and (3.10) to rewrite the low-$\beta_{\rm p}$ heating rate in (3.7) in terms of δ and $v_{\rm A}$. We then add the low-$\beta_{\rm p}$ heating rate to the high-$\beta_{\rm p}$ heating rate in (3.8), obtaining

$$\frac{Q_\perp}{\Omega v_{\rm A}^2} = \sigma_1 \delta^3 \exp\left(-\frac{\sigma_2}{\delta}\right) + \frac{1.69 c_1 \delta^3}{\beta_{\rm p}^{1/2}} \exp\left(-\frac{0.84 c_2 \beta_{\rm p}^{1/2}}{\delta}\right). \tag{3.11}$$

The first term on the right-hand side dominates at $\beta_{\rm p} \gtrsim 1$ in part because $\sigma_1 \simeq 6.5 c_1$. The second term on the right-hand side dominates at $\beta_{\rm p} \ll 1$. Figure 4 shows that (3.11) is consistent with our numerical results. This figure also illustrates how, at fixed $\delta B_\rho/B_0$, the stochastic-heating rate increases as $\beta_{\rm p}$ decreases.

As mentioned above, stochastic heating becomes more effective as the fluctuations become more intermittent (Xia *et al.* 2013; Mallet *et al.* 2018). The randomly phased waves in our test-particle simulations are not intermittent, but gyroscale fluctuations in space and astrophysical plasmas generally are (see, e.g. Mangeney *et al.* 2001; Carbone *et al.* 2004; Salem *et al.* 2009; Chandran, Schekochihin & Mallet 2015; Mallet, Schekochihin & Chandran 2015). Further work is needed to determine how the best-fit constants in (3.5) and (3.6) depend upon the degree of intermittency at the proton gyroradius scale. Until this dependency is determined, some caution should be exercised when applying (3.11) to space and astrophysical plasmas. For reference, Bourouaine & Chandran (2013) found that lowering c_2 to $\simeq$0.2 led the heating rate in (2.41) to be consistent with the proton-heating rate and fluctuation amplitudes inferred from measurements of the fast solar wind from the Helios spacecraft at $r = 0.3$ au. However, if $c_2 = 0.33$, then the heating rate in (2.41) is too weak to explain the proton heating seen in the Helios measurements.

4. Summary

In this paper we use phenomenological arguments to derive an analytic formula for the rate at which thermal protons are stochastically heated by AW/KAW turbulence at

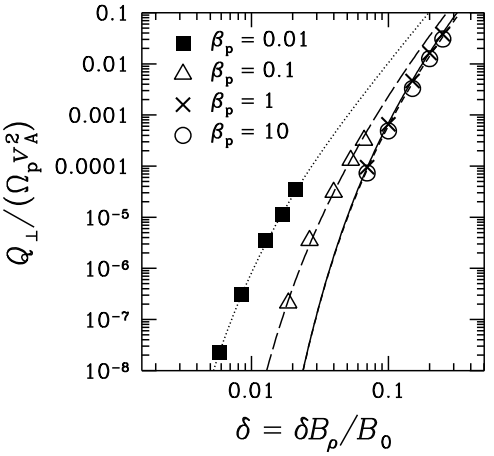

FIGURE 4. The data points reproduce the numerical results from figure 3 for $\beta_p = 0.01$, 0.1, 1.0 and 10. The dotted, long-dashed, solid and short-dashed lines plot (3.11) for, respectively, $\beta_p = 0.01$, $\beta_p = 0.1$, $\beta_p = 1$ and $\beta_p = 10$. The solid and short-dashed lines are difficult to distinguish because they are nearly on top of each other.

$k_\perp \rho_{th} \sim 1$. We focus on $\beta_p \sim 1 - 30$. Smaller values of β_p were considered by Chandran *et al.* (2010). At larger values of β_p, KAWs at $k_\perp \rho_{th} \sim 1$ become non-propagating, and some of the scalings we have assumed do not apply. At $\beta_p \sim 1 - 30$, the motion of a proton's effective guiding centre is dominated by the interaction between the proton and gyroscale fluctuations in the magnetic field, whose amplitude is denoted δB_ρ. As $\delta B_\rho / B_0$ increases from infinitesimal values towards unity, the proton motion in the plane perpendicular to $\boldsymbol{B}_0$ becomes random (stochastic), leading to spatial diffusion, and this spatial diffusion breaks the strong correlation between changes in a proton's perpendicular kinetic energy and the magnetic-field strength at the proton's location that normally gives rise to magnetic-moment conservation. The interaction between the proton and the electric field then becomes a Markov process that causes the proton to diffuse in energy. This energy diffusion leads to heating. At $\beta_p \sim$ 1–30, it is the solenoidal component of the electric field that dominates the heating.

The analytic formula that we derive for the stochastic heating rate $Q_\perp$ contains two dimensionless constants, σ_1 and σ_2, whose values depend upon the nature of the AW/KAW fluctuations with which the proton interacts (e.g. randomly phased waves or intermittent turbulence). We numerically track test particles interacting with randomly phased AWs and KAWs and find that our analytic formula for $Q_\perp$ agrees well with the heating rate of these test particles for the choices $\sigma_1 = 5.0$ and $\sigma_2 = 0.21$. We note that previous work has shown that for fixed r.m.s. amplitudes of the gyroscale fluctuations, stochastic heating is more effective when protons interact with intermittent turbulence than when protons interact with randomly phased waves (Chandran *et al.* 2010; Xia *et al.* 2013; Mallet *et al.* 2018). The reason for this is that in intermittent turbulence, most of the heating occurs near coherent structures, in which the fluctuation amplitudes are larger than average and in which the particle orbits are more stochastic than on average.

Our work leaves a number of interesting questions unanswered. Two such questions are how the energy-diffusion coefficient depends on energy at $\beta_p \sim 1 - 30$ and how the proton distribution function evolves in the presence of stochastic heating.

(For a discussion of the low-$\beta_{\rm p}$ case, see Klein & Chandran (2016).) We also have not addressed the question of how stochastic heating changes as $\beta_{\rm p}$ is increased to values $\gtrsim 30$ and KAWs at $k_\perp \rho_{\rm th} \sim 1$ become non-propagating, or how the stochastic-heating rate for minor ions depends upon minor-ion mass, charge and average flow speed along $\boldsymbol{B}_0$ in the proton frame. (For a discussion of the low-$\beta_{\rm p}$ case, see Chandran *et al.* (2013).) Previous studies have compared observationally inferred heating rates in the solar wind with the low-$\beta_{\parallel \rm p}$ stochastic-heating rate in (2.41) derived by Chandran *et al.* (2010), finding quantitative agreement at $r = 0.3$ au assuming $c_2 \simeq 0.2$ (Bourouaine & Chandran 2013) and qualitative agreement at $r = 1$ au (Vech, Klein & Kasper 2017). However, it is not yet clear whether the stochastic-heating rate in (2.40) agrees with solar-wind measurements in the large-$\beta_{\parallel \rm p}$ regime. In addition, stochastic heating at $\beta_{\parallel \rm p} \gtrsim 1$ could trigger temperature-anisotropy instabilities, which could in turn modify the rate(s) of perpendicular (and parallel) proton heating. Future investigations of these questions will be important for determining more accurately the role of stochastic heating in space and astrophysical plasmas.

Acknowledgements

We thank L. Arzamasskiy, Y. Kawazura, M. Kunz, E. Quataert and A. Schekochihin for valuable discussions. This work was supported in part by NASA grants NNX15AI80, NNX16AG81G, NNS16AM23G, NNX17AI18G, and NNN06AA01C and NSF grant PHY-1500041. D.V. acknowledges the support of STFC Ernest Rutherford Fellowship ST/P003826/1.

Appendix A. Non-propagation of KAWs at $k_\perp \rho_{\rm th} \sim 1$ at high $\beta_{\rm p}$

In figure 5, we compare the AW/KAW dispersion relation from the two-fluid model of Hollweg (1999) and the PLUME hot-plasma-dispersion-relation solver (Klein & Howes 2015) for $T_{\rm e}/T_{\rm p} = 0.5$ and $v_{\rm A}/c = 0.003$ and for various values of $\beta_{\rm p}$. The PLUME results shown here assume that $k_\parallel \rho_{\rm th} = 0.001$ and that the proton and electron distributions are Maxwellian. The two-fluid dispersion relation agrees reasonably well with the more accurate PLUME results at $\beta_{\rm p} \lesssim 1$. However, at $\beta_{\rm p} \gtrsim 1$, the PLUME results deviate from the two-fluid theory because of ion damping, which becomes stronger as $\beta_{\rm p}$ increases (Howes *et al.* 2008; Kunz *et al.* 2018). Starting at $\beta_{\rm p} \simeq 30$ (for $T_{\rm e}/T_{\rm p} = 0.5$, $v_{\rm A}/c = 0.003$ and $k_\parallel \rho_{\rm p} = 0.001$), the real part (but not the imaginary part) of the KAW frequency at $k_\perp \rho_{\rm th} = 1$ vanishes (i.e. KAWs become damped, non-propagating modes). For larger $\beta_{\rm p}$ values, KAWs are non-propagating throughout an interval of $k_\perp \rho_{\rm th}$ values centred on unity that broadens to both larger and smaller values as $\beta_{\rm p}$ increases (Kawazura *et al.* 2018).

Appendix B. Stochastic heating by the electrostatic potential at $\beta_{\rm p} \gtrsim 1$

In § 2 we considered the r.m.s. change to a thermal proton's energy ΔH resulting from the solenoidal component of the electric field $\boldsymbol{E}_{\rm s}$ during the particle residence time Δt within one set of gyroscale eddies. We also evaluated the contribution of $\boldsymbol{E}_{\rm s}$ to the stochastic heating rate $Q_\perp$. Here, we show that the contribution to $Q_\perp$ from $\boldsymbol{E}_{\rm s}$ is larger than the contribution from the electrostatic potential Φ when $\beta_{\rm p} \gtrsim 1$.

We assume that the r.m.s. amplitude of the potential part of the electric field at $k_\perp \rho_{\rm th}$ is comparable to the r.m.s. amplitude of the total gyroscale electric-field fluctuation, δE_ρ, which in turn is $\sim \delta v_\rho B_0/c$. As discussed by Chandran *et al.* (2010), the contribution of the time-varying electrostatic potential to ΔH is

$$\Delta H_{\rm potential} \sim q \omega_{\rm eff} \Delta \Phi_\rho \Delta t, \tag{B 1}$$

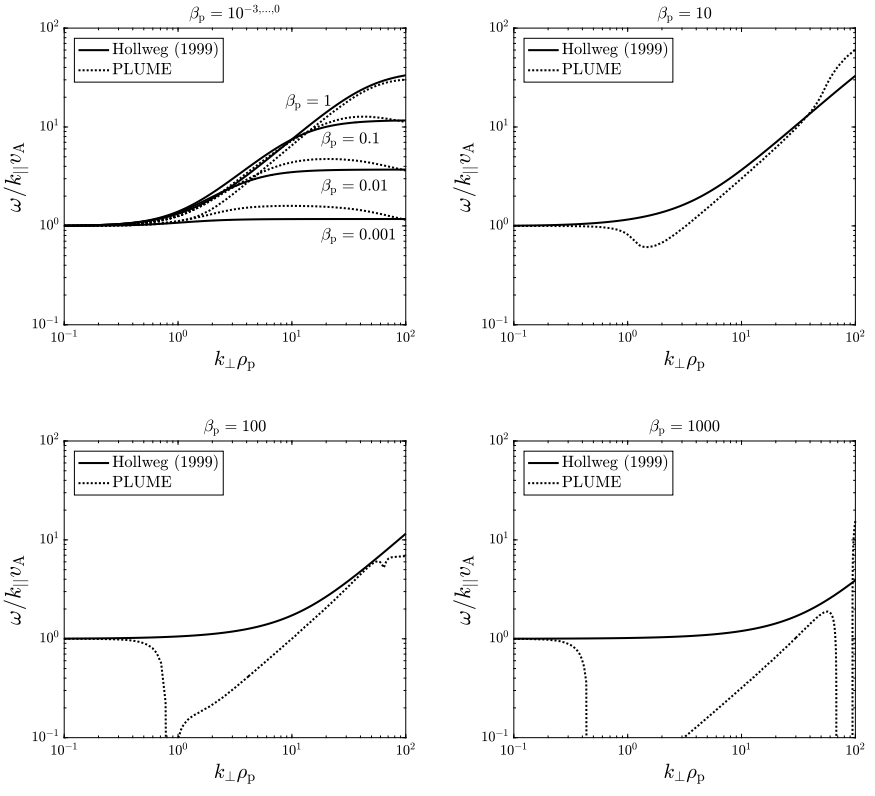

FIGURE 5. The KAW dispersion relation from Hollweg's (1999) two-fluid model (solid lines) and the PLUME hot-plasma-dispersion-relation solver (Klein & Howes 2015) (dotted lines) for $T_e/T_p = 0.5$ and $v_A/c = 0.003$ for various powers of β_p.

where $\omega_{\rm eff} = \delta v_\rho/\rho_{\rm th}$ (see (2.35)), and

$$q\Delta\Phi_\rho \sim q\rho_{\rm th}\delta E_\rho \sim qw_\perp \times \frac{mc}{qB_0} \times \frac{\delta v_\rho B_0}{c} \sim mw_\perp \delta v_\rho. \tag{B 2}$$

Since (2.27) gives $\Delta t \sim \beta_p^{-1/2}\rho_{\rm th}/\delta v_\rho$,

$$\omega_{\rm eff}\Delta t \sim \beta_p^{-1/2}. \tag{B 3}$$

Combining (B 1) through (B 3), we obtain

$$\Delta H_{\rm potential} \sim \beta_p^{-1/2} mw_\perp \delta v_\rho, \tag{B 4}$$

$$D_{K,\rm potential} \sim \frac{(\Delta H_{\rm potential})^2}{\Delta t} \sim \frac{\beta_p^{-1} m^2 w_\perp^2 (\delta v_\rho)^2}{\beta_p^{-1/2}\rho_{\rm th}/\delta v_\rho} \sim \beta_p^{-1/2} m^2 w_\perp^2 \frac{(\delta v_\rho)^3}{\rho_{\rm th}}, \tag{B 5}$$

and

$$Q_{\perp,\rm potential} \sim \frac{D_{K,\rm potential}}{mK_\perp} \sim \beta_p^{-1/2}\frac{(\delta v_\rho)^3}{\rho_{\rm th}}, \tag{B 6}$$

which is a factor of $\sim\beta_p^{-1}$ smaller than the estimate of $Q_\perp$ in (2.39).

REFERENCES

BALE, S. D., KELLOGG, P. J., MOZER, F. S., HORBURY, T. S. & REME, H. 2005 Measurement of the electric fluctuation spectrum of magnetohydrodynamic turbulence. *Phys. Rev. Lett.* **94** (21), 215002.

BELCHER, J. W. 1971 ALFVÉNIC wave pressures and the solar wind. *Astrophys. J.* **168**, 509.

BORIS, J. P. 1970 Relativistic plasma simulation-optimization of a hybrid code. In *Proceeding of Fourth Conference on Numerical Simulations of Plasmas*.

BOUROUAINE, S. & CHANDRAN, B. D. G. 2013 Observational test of stochastic heating in low-β fast-solar-wind streams. *Astrophys. J.* **774**, 96, arXiv:1307.3789.

CARBONE, V., BRUNO, R., SORRISO-VALVO, L. & LEPRETI, F. 2004 Intermittency of magnetic turbulence in slow solar wind. *Planet. Space Sci.* **52**, 953–956.

CHANDRAN, B., VERSCHAREN, D., QUATAERT, E., KASPER, C., ISENBERG, P. & BOUROUAINE, B. 2013 Stochastic heating, differential flow, and the alpha-to-proton temperature ratio in the solar wind. *Astrophys. J.* **776**, 45.

CHANDRAN, B. D. G., DENNIS, T. J., QUATAERT, E. & BALE, S. D. 2011 Incorporating kinetic physics into a two-fluid solar-wind model with temperature anisotropy and low-frequency Alfvén-wave turbulence. *Astrophys. J.* **743**, 197, arXiv:1110.3029.

CHANDRAN, B. D. G., LI, B., ROGERS, B. N., QUATAERT, E. & GERMASCHEWSKI, K. 2010 Perpendicular ion heating by low-frequency Alfvén-wave turbulence in the solar wind. *Astrophys. J.* **720**, 503–515.

CHANDRAN, B. D. G., SCHEKOCHIHIN, A. A. & MALLET, A. 2015 Intermittency and alignment in strong RMHD turbulence. *Astrophys. J.* **807**, 39, arXiv:1403.6354.

CHASTON, C. C., BONNELL, J. W., CARLSON, C. W., MCFADDEN, J. P., ERGUN, R. E., STRANGEWAY, R. J. & LUND, E. J. 2004*a* Auroral ion acceleration in dispersive Alfvén waves. *J. Geophys. Res. Phys.* **109** (A4), a04205.

CHASTON, C. C., BONNELL, J. W., CARLSON, C. W., MCFADDEN, J. P., ERGUN, R. E., STRANGEWAY, R. J. & LUND, E. J. 2004*b* Auroral ion acceleration in dispersive Alfvén waves. *J. Geophys. Res. (Space Phys.)* **109**, 4205.

CHEN, C. H. K. 2016 Recent progress in astrophysical plasma turbulence from solar wind observations. *J. Plasma Phys.* **82** (6), 535820602.

CHEN, L., LIN, Z. & WHITE, R. 2001*a* On resonant heating below the cyclotron frequency. *Phys. Plasmas* **8** (11), 4713–4716.

CHEN, L., LIN, Z. & WHITE, R. 2001*b* On resonant heating below the cyclotron frequency. *Phys. Plasmas* **8**, 4713–4716.

CHO, J. & LAZARIAN, A. 2004 The anisotropy of electron magnetohydrodynamic turbulence. *Astrophys. J. Lett.* **615**, L41–L44.

CHO, J. & VISHNIAC, E. T. 2000 The anisotropy of magnetohydrodynamic Alfvénic turbulence. *Astrophys. J.* **539**, 273–282.

COLEMAN, P. J. JR. 1968 Turbulence, viscosity, and dissipation in the solar–wind plasma. *Astrophys. J.* **153**, 371.

CRANMER, S. R., VAN BALLEGOOIJEN, A. A. & EDGAR, R. J. 2007 Self-consistent coronal heating and solar wind acceleration from anisotropic magnetohydrodynamic turbulence. *Astrophys. J. Suppl.* **171**, 520–551.

CRANMER, S. R., MATTHAEUS, W. H., BREECH, B. A. & KASPER, J. C. 2009 Empirical constraints on proton and electron heating in the fast solar wind. *Astrophys. J.* **702**, 1604–1614.

DE PONTIEU, B., MCINTOSH, S. W., CARLSSON, M., HANSTEEN, V. H., TARBELL, T. D., SCHRIJVER, C. J., TITLE, A. M., SHINE, R. A., TSUNETA, S., KATSUKAWA, Y. *et al.* 2007 Chromospheric alfvénic waves strong enough to power the solar wind. *Science* **318** (5856), 1574–1577.

DMITRUK, P., MATTHAEUS, W. H. & SEENU, N. 2004 Test particle energization by current sheets and nonuniform fields in magnetohydrodynamic turbulence. *Astrophys. J.* **617**, 667–679.

DURNEY, B. R. 1972 Solar-wind properties at the earth as predicted by one-fluid models. *J. Geophys. Res.* **77** (22), 4042–4051.

ESSER, R., FINESCHI, S., DOBRZYCKA, D., HABBAL, S. R., EDGAR, R. J., RAYMOND, J. C., KOHL, J. L. & GUHATHAKURTA, M. 1999 Plasma properties in coronal holes derived from measurements of minor ion spectral lines and polarized white light intensity. *Astrophys. J. Lett.* **510** (1), L63.

FIKSEL, G., ALMAGRI, A. F., CHAPMAN, B. E., MIRNOV, V. V., REN, Y., SARFF, J. S. & TERRY, P. W. 2009 Mass-dependent ion heating during magnetic reconnection in a laboratory plasma. *Phys. Rev. Lett.* **103** (14), 145002.

GOLDREICH, P. & SRIDHAR, S. 1995 Toward a theory of interstellar turbulence. 2: strong Alfvénic turbulence. *Astrophys. J.* **438**, 763–775.

GROŠELJ, D., CERRI, S. S., BAÑÓN NAVARRO, A., WILLMOTT, C., TOLD, D., LOUREIRO, N. F., CALIFANO, F. & JENKO, F. 2017 Fully kinetic versus reduced-kinetic modeling of collisionless plasma turbulence. *Astrophys. J.* **847**, 28, arXiv:1706.02652.

HARTLE, R. E. & STURROCK, P. A. 1968 Two-fluid model of the solar wind. *Astrophys. J.* **151**, 1155.

HAUFF, T., JENKO, F., SHALCHI, A. & SCHLICKEISER, R. 2010 Scaling theory for cross-field transport of cosmic rays in turbulent fields. *Astrophys. J.* **711**, 997–1007.

HELLINGER, P. & MATSUMOTO, H. 2000 New kinetic instability: oblique Alfvén fire hose. *J. Geophys. Res.* **105**, 10519–10526.

HELLINGER, P., TRÁVNÍČEK, P. M., ŠTVERÁK, Š., MATTEINI, L. & VELLI, M. 2013 Proton thermal energetics in the solar wind: helios reloaded. *J. Geophys. Res. (Space Phys.)* **118**, 1351–1365.

HOLLWEG, J. V. 1999 Kinetic alfvén wave revisited. *J. Geophys. Res.* **104** (A7), 14811–14819.

HOLLWEG, J. V. & ISENBERG, P. A. 2002 Generation of the fast solar wind: a review with emphasis on the resonant cyclotron interaction. *J. Geophys. Res. (Space Phys.)* **107**, 1147.

HORBURY, T. S., FORMAN, M. & OUGHTON, S. 2008 Anisotropic scaling of magnetohydrodynamic turbulence. *Phys. Rev. Lett.* **101** (17), 175005.

HOWES, G. G., COWLEY, S. C., DORLAND, W., HAMMETT, G. W., QUATAERT, E. & SCHEKOCHIHIN, A. A. 2008 A model of turbulence in magnetized plasmas: implications for the dissipation range in the solar wind. *J. Geophys. Res. (Space Phys.)* **113**, A05103.

HUGHES, R. S., GARY, S. P., WANG, J. & PARASHAR, T. N. 2017 Kinetic Alfvén turbulence: electron and ion heating by particle-in-cell simulations. *Astrophys. J. Lett.* **847**, L14.

VAN DER HOLST, B., SOKOLOV, I. V., MENG, X., JIN, M., MANCHESTER, W. B. IV, TÓTH, G. & GOMBOSI, T. I. 2014 Alfvén wave solar model (AWSoM): coronal heating. *Astrophys. J.* **782**, 81, arXiv:1311.4093.

JOHNSON, J. R. & CHENG, C. Z. 2001 Stochastic ion heating at the magnetopause due to kinetic Alfvén waves. *Geophys. Res. Lett.* **28**, 4421–4424.

KAWAZURA, Y., BARNES, M. & SCHEKOCHIHIN, A. A. 2018 Thermal disequilibration of ions and electrons by collisionless plasma turbulence. ArXiv e-prints, arXiv:1807.07702.

KLEIN, K. G. & CHANDRAN, B. D. G. 2016 Evolution of the proton velocity distribution due to stochastic heating in the near-sun solar wind. *Astrophys. J.* **820**, 47, arXiv:1602.05114.

KLEIN, K. G. & HOWES, G. G. 2015 Predicted impacts of proton temperature anisotropy on solar wind turbulence. *Phys. Plasmas* **22** (3), 032903.

KRUSKAL, M. 1962 Asymptotic theory of Hamiltonian and other systems with all solutions nearly periodic. *J. Math. Phys.* **3**, 806–828.

KUNZ, M. W., ABEL, I. G., KLEIN, K. G. & SCHEKOCHIHIN, A. A. 2018 Astrophysical gyrokinetics: turbulence in pressure-anisotropic plasmas at ion scales and beyond. *J. Plasma Phys.* **84** (2), 715840201.

LEHE, R., PARRISH, I. J. & QUATAERT, E. 2009 The heating of test particles in numerical simulations of Alfvénic turbulence. *Astrophys. J.* **707**, 404–419.

LYNN, J. W., PARRISH, I. J., QUATAERT, E. & CHANDRAN, B. D. G. 2012 Resonance broadening and heating of charged particles in magnetohydrodynamic turbulence. *Astrophys. J.* **758** (2), 78.

MALLET, A., KLEIN, K. G., CHANDRAN, B. D. G., GROSELJ, D., HOPPOCK, I. W., BOWEN, T. A., SALEM, C. S. & BALE, S. D. 2018 Interplay between intermittency and dissipation in collisionless plasma turbulence, ArXiv e-prints, arXiv:1807.09301.

MALLET, A., SCHEKOCHIHIN, A. A. & CHANDRAN, B. D. G. 2015 Refined critical balance in strong Alfvénic turbulence. *Mon. Not. R. Astron. Soc.* **449**, L77–L81.

MANGENEY, A., SALEM, C., VELTRI, P. L. & CECCONI, B. 2001 Intermittency in the solar wind turbulence and the haar wavelet transform. In *Sheffield Space Plasma Meeting: Multipoint Measurements Versus Theory* (ed. B. Warmbein), vol. 492, p. 53. ESA Special Publication.

MARKOVSKII, S. A., VASQUEZ, B. J., SMITH, C. W. & HOLLWEG, J. V. 2006 Dissipation of the perpendicular turbulent cascade in the solar wind. *Astrophys. J.* **639** (2), 1177.

MARSCH, E. 2006 Kinetic physics of the solar corona and solar wind. *Living Rev. Solar Phys.* **3**, 1.

MCCHESNEY, J. M., STERN, R. A. & BELLAN, P. M. 1987 Observation of fast stochastic ion heating by drift waves. *Phys. Rev. Lett.* **59**, 1436–1439.

NORTHROP, T. G. 1963 *The Adiabatic Motion of Charged Particles*. Interscience.

PARKER, E. N. 1958 Dynamics of the interplanetary gas and magnetic fields. *Astrophys. J.* **128**, 664.

PARKER, E. N. 1965 Dynamical theory of the solar wind. *Space Sci. Rev.* **4**, 666–708.

PODESTA, J. J. 2013 Evidence of kinetic Alfvén waves in the solar wind at 1 AU. *Solar Phys.* **286**, 529–548.

QUATAERT, E. 1998 Particle heating by Alfvénic turbulence in hot accretion flows. *Astrophys. J.* **500**, 978–991.

SALEM, C., MANGENEY, A., BALE, S. D. & VELTRI, P. 2009 Solar wind magnetohydrodynamics turbulence: anomalous scaling and role of intermittency. *Astrophys. J.* **702**, 537–553.

SCHEKOCHIHIN, A. A., COWLEY, S. C., DORLAND, W., HAMMETT, G. W., HOWES, G. G., QUATAERT, E. & TATSUNO, T. 2009 Astrophysical gyrokinetics: kinetic and fluid turbulent cascades in magnetized weakly collisional plasmas. *Astrophys. J. Suppl.* **182** (1), 310.

SERVIDIO, S., GRECO, A., MATTHAEUS, W. H., OSMAN, K. T. & DMITRUK, P. 2011 Statistical association of discontinuities and reconnection in magnetohydrodynamic turbulence. *J. Geophys. Res.* **116** (A9), a09102.

SHEBALIN, J. V., MATTHAEUS, W. H. & MONTGOMERY, D. 1983 Anisotropy in MHD turbulence due to a mean magnetic field. *J. Plasma Phys.* **29**, 525–547.

TENBARGE, J. M., PODESTA, J. J., KLEIN, K. G. & HOWES, G. G. 2012 Interpreting magnetic variance anisotropy measurements in the solar wind. *Astrophys. J.* **753**, 107, arXiv:1205.0749.

TOMCZYK, S., MCINTOSH, S. W., KEIL, S. L., JUDGE, P. G., SCHAD, T., SEELEY, D. H. & EDMONDSON, J. 2007 Alfvén waves in the solar corona. *Science* **317** (5842), 1192–1196.

TU, C.-Y. & MARSCH, E. 1995 MHD structures, waves and turbulence in the solar wind: observations and theories. *Space Sci. Rev.* **73**, 1–210.

VECH, D., KLEIN, K. G. & KASPER, J. C. 2017 Nature of stochastic ion heating in the solar wind: testing the dependence on plasma beta and turbulence amplitude. *Astrophys. J. Lett.* **850**, L11, arXiv:1711.01508.

VECH, D., KLEIN, K. G. & KASPER, J. C. 2018 Large-scale control of kinetic dissipation in the solar wind. *Astrophys. J. Lett.* **863**, L4, arXiv:1807.04773.

VERDINI, A., VELLI, M., MATTHAEUS, W. H., OUGHTON, S. & DMITRUK, P. 2010 A turbulence-driven model for heating and acceleration of the fast wind in coronal holes. *Astrophys. J. Lett.* **708**, L116–L120.

WU, P., WAN, M., MATTHAEUS, W. H., SHAY, M. A. & SWISDAK, M. 2013 von Kármán energy decay and heating of protons and electrons in a kinetic turbulent plasma. *Phys. Rev. Lett.* **111** (12), 121105.

XIA, Q., PEREZ, J. C., CHANDRAN, B. D. G. & QUATAERT, E. 2013 Perpendicular ion heating by reduced magnetohydrodynamic turbulence. *Astrophys. J.* **776**, 90, arXiv:1309.0742.